Kirenol relieves rheumatoid arthritis by targeting the TWEAK/Fn14 pathway

ZIXIN CHEN[1*], JINXUAN WANG[2*], LIJUAN XIAO[1*], ZHIHUI CHEN[1], WENCHUAN LUO[1], WEN XU[1], YA LIN[1], MEI HUANG[1], YUQIAN ZHANG[1], YINGHAO WANG[1], YAPING CHEN[1] and LIHONG NAN[1]

[1]College of Pharmacy, Fujian University of Traditional Chinese Medicine, Fuzhou, Fujian 350122, P.R. China;
[2]School of Basic Medical Sciences, Fujian Medical University, Fuzhou, Fujian 350004, P.R. China

Received January 26, 2025; Accepted June 2, 2025

DOI: 10.3892/ijmm.2025.5586

Abstract. Fibroblast-like synoviocytes (FLSs) are the primary drivers of synovial tissue hyperplasia in rheumatoid arthritis (RA). Activation of the tumor necrosis factor-like weak inducer of apoptosis (TWEAK)/fibroblast growth factor-inducible immediate-early response protein 14 (Fn14) pathway significantly contributes to the pathogenesis of RA. Kirenol (Kir), a compound with anti-inflammatory and anti-rheumatic properties, has an unclear mechanism of action. To comprehensively investigate the effects and potential mechanisms of Kir on RA, the present study employed both an *in vitro* model of transforming growth factor-β1 (TGF-β1)-induced human fibroblast-like MH7A synoviocytes proliferation and an *in vivo* collagen-induced arthritis (CIA) rat model. The effects of Kir on synovial fibroblasts were detected via flow cytometry, ELISA, hematoxylin and eosin staining, safranin-O/fast green staining, immunohistochemistry, immunofluorescence and western blotting. Kir ameliorated pathological damage in the synovial tissue of CIA rats, suppressed rheumatoid factor production, regulated the T helper 17 cells/regulatory T cell balance and mitigated joint inflammation and swelling. Additionally, Kir markedly downregulated the protein levels of the TWEAK/Fn14 pathway in synovial tissue. Surface plasmon resonance demonstrated that Kir could specifically bind to Fn14. Kir significantly suppressed the TGF-β1-mediated aberrant proliferation and migration of MH7A cells. However, the overexpression of Fn14 reversed the inhibitory effects of Kir on the abnormal proliferation and migration of cells, as did the activation of the TWEAK/Fn14 pathway. These results suggest that Kir possesses anti-RA properties by inhibiting abnormal immune-inflammatory responses, as well as synovial cell proliferation and migration. These effects of Kir may be linked to a decrease in the activity of the TWEAK/Fn14 pathway.

Correspondence to: Professor Lihong Nan or Dr Yaping Chen, College of Pharmacy, Fujian University of Traditional Chinese Medicine, 1 Qiuyang Road, Fuzhou, Fujian 350122, P.R. China
Email: nlhong1152@163.com
Email: zlchenyaping@126.com

*Contributed equally

Key words: rheumatoid arthritis, kirenol, tumor necrosis factor-like weak inducer of apoptosis, fibroblast growth factor-inducible immediate-early response protein 14, synovial fibroblast

Introduction

Rheumatoid arthritis (RA), a chronic autoimmune disorder marked by progressive joint inflammation, is characterized by high disability rates and it severely impacts the quality of life of patients (1-3). The incidence of RA shows a progressive increase as age advances (4). Aberrant activation of the immune system in RA leads to chronic inflammation of the synovium. This inflammation leads to pathological changes, including synovial hyperplasia, infiltration of inflammatory cells and invasion of synovial cells into the cartilage and subchondral bone, ultimately resulting in joint destruction (5). Fibroblast-like synoviocytes (FLSs) are the primary effector cells that drive synovial tissue proliferation and inflammation in RA. The inflammatory factors and cytokines produced by activated FLSs are pivotal in the pathogenesis of RA synovial inflammation, contributing to both the initiation and progression of the disease (6). Activated FLSs produce inflammatory factors and matrix metalloproteinases (MMPs), which recruit immune cells (such as macrophages, T lymphocytes and neutrophils) and contribute to cytokine imbalances. This further exacerbates FLS activation, driving synovial hyperplasia and inflammation, culminating in the continuous degradation of the cartilage matrix, leading to the destruction of both cartilage and bone (7,8).

Tumor necrosis factor-like weak inducer of apoptosis (TWEAK) is a novel arthritis mediator. Fibroblast growth factor-inducible immediate-early response protein 14 (Fn14) serves as the specific receptor for TWEAK. This interaction triggers cytokine secretion, promotes synoviocytes proliferation and migration as well as modulates immunity, significantly contributing to the progression of RA (9-12).

The precise pathogenesis of RA remains incompletely understood and no effective treatment exists yet; however, early treatment with medications can significantly reduce symptoms

and slow the progression of RA. Paradoxically, first-line agents encompass non-steroidal anti-inflammatory drugs (NSAIDs), disease-modifying antirheumatic drugs (DMARDs), biological response modifiers and glucocorticoids, which exhibit significant long-term risks, including gastrointestinal damage, hepatotoxicity, cardiovascular complications and renal impairment, which collectively constrain their therapeutic sustainability (13-15). The traditional Chinese herbal medicine, Sigesbeckia herba, has been employed for the treatment of arthritis for centuries and its safety and efficacy are documented through a long history of human use (16,17). Kirenol (Kir), a labdane-type diterpenoid, is the primary bioactive ingredient of Siegesbeckia herba. It has been reported that Kir exerts a potent anti-arthritic effect in collagen-induced arthritis by modifying the T cell balance (18). Kir upregulates nuclear annexin-1 and inhibits NF-κB activation in attenuating synovial inflammation of collagen-induced arthritis (CIA) rats (19). It has also been reported that Kir can significantly inhibit PI3K/Akt activation and exert a protective effect on mouse osteoarthritis models (20).

Kir also demonstrates rapid absorption kinetics in the rat intestinal tract, with oral bioavailability and a favorable safety profile observed during preclinical pharmacokinetic and toxicological evaluations (21). Unlike glucocorticoids, Kir maintains therapeutic effects without suppressing the adrenocorticotropic hormone or downregulating the glucocorticoid receptor pathways, and Kir is less likely to evoke therapy resistance and the resulting adverse reactions (19).

However, the specific signaling pathways and molecular targets mediating the effects of Kir on RA remains to be fully elucidated. Therefore, the present study used a CIA rat model and transforming growth factor-β1 (TGF-β1)-induced human FLSs (MH7A cells) to investigate the involvement of the TWEAK/Fn14 pathway in mediating the anti-RA effect of Kir. The findings offer new insights and experimental evidence for the treatment of RA, as well as the identification of potential candidate drugs for RA therapy.

Materials and methods

Materials. Kir (lot no. HR1386W3; purity ≥98%) was purchased from Baoji Herbest Bio-Tech Co., Ltd.; bovine type II collagen, complete Freund's adjuvant (CFA) and incomplete Freund's adjuvant (cat. nos. 20022, 7001 and 7002, respectively) were produced by Chondrex, Inc.; TGF-β1 (cat. no. 100-21) was purchased from PeproTech, Inc.; hematoxylin and eosin (H&E) staining kit (cat. no. G1120) and safranin-O/fast green staining kit (cat. no. G1371) were produced by Beijing Solarbio Science & Technology Co., Ltd.; Cell Counting Kit-8 (CCK-8; cat. no. C0005-10) was produced by Shanghai Topscience Biotech Co., Ltd. (Shandong Zhongshan Biotechnology Co., Ltd.); the human Fn14-overexpressing lentivirus (Fn14-OE; lot no. LV81072534) and negative control lentivirus (NC; lot no. LV81072533) were synthesized by Hanheng Biotechnology (Shanghai) Co., Ltd. Details of the ELISA kits and antibodies used in the study are listed in Tables I and II.

Preparation of the CIA rat model and animal experimental procedure. SPF-grade male SD rats (180±20 g, 6 weeks old) were acquired from Shanghai SLAC Laboratory Animal Co. Ltd. [production license: SCXK (Shanghai) 2022-0004]. All animals were maintained on a 12/12 h light/dark cycle (lights on at 6:00 a.m., lights off: at 6:00 p.m.) in an environmentally controlled breeding room (temperature, 20-25˚C; relative humidity, 45-55%) with access to sterile pellet food and water *ad libitum*. Rats were monitored daily for weight loss and overall health condition and were euthanized upon reaching the humane endpoints (inability to obtain feed or water and/or a loss of >20% of body weight). No rats reached these humane endpoints. All animal experiments were carried out in strict accordance with the ARRIVE guidelines, and the animal procedures were approved by the Animal Ethics Committee of Fujian University of Traditional Chinese Medicine (Fuzhou, China; approval no. FJTCM IACUC 2023008). In total, 10 rats were randomly allocated to the control group, and the remaining 55 rats were utilized to establish a CIA model. CIA model preparation followed the methodology outlined in our previous study (22). Briefly, type II collagen (2 mg/ml) was emulsified with an equal volume of CFA or incomplete Freund's adjuvant on ice. Briefly, each rat was subcutaneously injected at the tail base with 0.2 ml of bovine type II collagen emulsion (with CFA), and secondary immunization was carried out via the administration of 0.1 ml of bovine type II collagen emulsion (with incomplete Freund's adjuvant) on the seventh day. The control rats received the same volume of normal saline injection at the tail base. All rats were scored according to the arthritis index (AI) (23): i) Mild redness and swelling of one or both ankle or knee joints, or close to redness and swelling spreading to the tips of the toes; ii) moderate redness and swelling of one or both ankle or knee joints; iii) severe redness and swelling of the entire paw, including the tips of the toes; and iv) the inability to bear weight. The scoring was independently conducted by two experienced evaluators who had no prior involvement in model preparation. Rats whose total limb AI scores were in the range of 6-12 were selected. In total, 5 rats that did not meet the criteria were excluded and euthanized. Thus, 50 rats were included, stratified and randomly divided into the CIA group, 1.25, 2.5 and 5 mg/kg Kir groups and the positive control group (21 mg/kg Pre), with 10 rats in each group. After successful modelling, Kir was administered intragastrically at 10 ml/kg. Rats in the control and CIA groups were administered saline. Treatment commenced once a day for 14 days (Fig. 1). The AI was recorded on the day of administration and every 3 days subsequently. The toe volume of the right posterior toe was measured using a volume measuring instrument before modelling, on the day of treatment initiation and every 3 days thereafter. Paw edema was calculated as follows: Paw edema=toe volume-baseline. The rats were anesthetized by intraperitoneal injection of 3% sodium pentobarbital (30 mg/kg) 2 h after the last administration, and blood was collected through the abdominal aorta. Then, the rats were euthanized by 5% isoflurane inhalation for 5 min using a small animal anesthesia machine (RWD Life Science Co., Ltd.). Synovial tissues were collected for analysis after death confirmation using standard criteria: Absent pulse and breathing, lost corneal reflexes, no response to deep toe stimulation and mucosal graying.

Table I. ELISA kits used in the present study.

ELISA kit	Supplier	Cat. no.
RF	Mlbio (Shanghai Enzyme-linked Biotechnology Co., Ltd.)	ml952541V
MMP-13	Wuhan Boster Biological Technology, Ltd.	EK0468
MCP-1	Wuhan Boster Biological Technology, Ltd.	EK0441
ICAM-1	Wuhan Boster Biological Technology, Ltd.	EK0370
CXCL-10	Wuhan Boster Biological Technology, Ltd.	EK0735
IL-10	Mlbio (Shanghai Enzyme-linked Biotechnology Co., Ltd.)	ml002813
IL-17	Chundubio (Wuhan Purity Biotechnology Co., Ltd.)	CD-JK30201

RF, rheumatoid factor; MMP-13, matrix metalloproteinase 13; MCP-1, monocyte chemoattractant protein-1; ICAM-1, intercellular adhesion molecule-1; CXCL-10, C-X-C motif C chemokine ligand-10; IL-17, interleukin 17; IL-10, interleukin 10.

Table II. Primary antibodies used in the present study.

Primary antibodies	Supplier	Cat. no.	Application/ dilution
CD4 Monoclonal Antibody (OX35) FITC	Thermo Fisher Scientific, Inc.	11-0040-82	FCM
CD25 Monoclonal Antibody (OX39) APC	Thermo Fisher Scientific, Inc.	17-0390-82	FCM
FOXP3 Monoclonal Antibody (FJK-16s) PE	Thermo Fisher Scientific, Inc.	12-5773-82	FCM
IL-17A Monoclonal Antibody (eBio17B7) PE	Thermo Fisher Scientific, Inc.	12-7177-81	FCM
MCP-1	Wuhan Servicebio Technology Co., Ltd.	GB11199	IHC/1:250
ICAM-1	Wuhan Servicebio Technology Co., Ltd.	GB11106	IHC/1:400
MMP-13	Wuhan Servicebio Technology Co., Ltd.	GB11247	IHC/1:200
CXCL-10	Abcam	ab9807	WB/1:500
CXCR3	ImmunoWay Biotechnology Company.	YT1161	WB/1:800
NF-κB p52	Thermo Fisher Scientific, Inc.	PA5-88086	IF/1:200 WB/1:1000
RelB	Santa Cruz Biotechnology, Inc.	Sc-48366	IF/1:200, WB/1:1000
TWEAK	ABclonal Biotech Co., Ltd.	A5659	WB/1:500
Fn14	Wuhan Boster Biological Technology, Ltd.	BM4635	WB/1:500
TRAF2	Cohesion Biosciences	CQA2285	WB/1:500
ASK1 (D11C9)	Cell Signaling Technology, Inc.	8662	WB/1:800
IKKα	ImmunoWay Biotechnology Company.	YT2302	WB/1:800
IKKα (phospho S176/177)	ImmunoWay Biotechnology Company.	YP0141	WB/1:800
NF-κB p100	ImmunoWay Biotechnology Company.	YT3093	WB/1:700
NF-κB p100 (phospho S869)	ImmunoWay Biotechnology Company.	YP0182	WB/1:700
IRE1	Proteintech Group, Inc.	27528-1-AP	WB/1:1000
IRE1 (phospho S724)	Abcam	ab48187	WB/1:1000
NIK	ImmunoWay Biotechnology Company.	YN1594	WB/1:800
β-actin	Proteintech Group, Inc.	66009-1	WB/1:10000
PCNA	Cohesion Biosciences	CPA9205	WB/1:2000

TWEAK, tumor necrosis factor-like weak inducer of apoptosis; Fn14, fibroblast growth factor-inducible immediate-early response protein 14; TRAF2, TNF receptor-associated factor 2; IKKα, inhibitor of κB kinase α; MCP-1, monocyte chemoattractant protein-1; ICAM-1, intercellular cell adhesion molecule-1; MMP-13, matrix metalloproteinases 13; CXCL10, C-X-C motif chemokine ligand 10; C-X-C motif chemokine receptor 3; NIK, nuclear factor-κB-inducing kinase; PCNA, proliferating cell nuclear antigen.

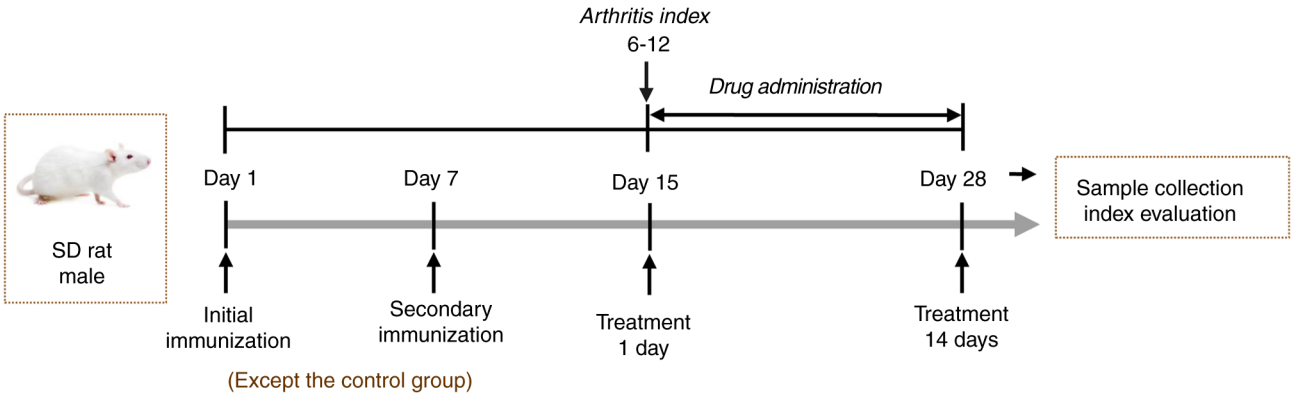

Figure 1. Schedule of the animal experiment.

Cell experimental procedures. The human MH7A RA synovial fibroblast cell line was sourced from iCell Bioscience, Inc. (Cellverse Co., Ltd.; lot no. iCell-Huh-008a). MH7A cells were maintained in DMEM (Wuhan Pricella Biotechnology Co., Ltd.; cat. no. PM150210) supplemented with 10% fetal bovine serum (FBS; Shanghai ExCell Biology, Inc.; cat. no. FSP500) and cultured in a 37˚C, 5% CO_2 incubator (Thermo Fisher Scientific, Inc.).

Effect of Kir on MH7A cell viability. MH7A cells were divided into the following groups: The control group (with complete DMEM) and the Kir intervention groups, with concentrations of 5, 10, 20, 40 and 80 μM.

TGF-β1-stimulated MH7A synovial fibroblast proliferation and drug intervention. MH7A cells were induced by 10 ng/ml TGF-β1 for 24 h at 37˚C to establish a model of MH7A cell proliferation. The cell groups were assigned as follows: The control group (untreated), TGF-β1 group, three Kir groups (TGF-β1 + 2.5, 5 or 10 μM Kir) and prednisone (Pre) group (TGF-β1 + 100 nM Pre). After 24 h of intervention at 37˚C, the optimal Kir concentration was determined through CCK-8 and scratch assays. This concentration was used for subsequent reverse validation experiments.

Reverse validation experiment. MH7A cells were transduced with Fn14-overexpressing lentivirus. The Fn14-OE or NC lentiviruses were generated in 293T cells [Hanheng Biotechnology (Shanghai) Co., Ltd.] co-transfected with two helper plasmids (10 μg psPAX2 and 10 μg pMD2.G) and pHBLV-CMV-TNFRSF12A-3FLAG-EF1-ZsGreen-T2A-PURO or pBLV-ZsGreen-PURO lentiviral vectors (10 μg) at room temperature (RT). The lentiviruses were collected twice at 24 and 48 h, respectively. The MH7A cells were cultured until their confluency reached 30-50%, then infected with lentivirus at MOI=3 in DMEM for 4 h. After 72 h, the efficiency of green fluorescent protein (GFP) expression was observed via fluorescence microscopy. After screening with 2 μg/ml puromycin [Hanheng Biotechnology (Shanghai) Co., Ltd.; cat. no. HB-PU-500], the stable cell lines were confirmed by western blot analysis. Then, after 24 h of TGF-β1 stimulation, the cells were randomly divided into the TGF-β1 group, Kir group (TGF-β1 + 5 μM Kir), Kir + Fn14- OE group (Fn14-OE MH7A cells + TGF-β1 + 5 μM Kir) and Kir + NC group (NC MH7A cells + TGF-β1 + 5 μM Kir). The control group included MH7A cells supplemented with complete DMEM.

Cell viability assay. After the MH7A cells were cultured, the viability was measured via the CCK-8 method. After the addition of CCK-8 solution in the dark for 2 h, optical density values at 450 nm were measured via a multifunctional microplate reader. The cell viability rate was measured relative to that of the control group and expressed as a percentage.

Scratch test. MH7A cells were cultured until their confluency reached nearly 80% in complete medium (10% FBS). After the TGF-β1 induction for 24 h, cells were washed with PBS and incubated in fresh medium containing 3% FBS. Equal-sized scratches were made vertically with a 10 μl lance tip at the position of the midline of each well, and drug intervention was conducted. The migration distance of the cells was observed and recorded at 0 and 8 h. The migration rate of the MH7A cells (%) was calculated as: (width of the scratch at time 0 h-width of the scratch at time 8 h)/width of the scratch at time 0 h x100%.

ELISA. Rheumatoid factor (RF), interleukin-17 (IL-17) and IL-10 in the serum, along with monocyte chemoattractant protein-1 (MCP-1), intercellular cell adhesion molecule-1 (ICAM-1), C-X-C motif chemokine ligand-10 (CXCL-10) and matrix metalloproteinase 13 (MMP-13) in the cell supernatant, were measured strictly following the ELISA kit instructions (Table I).

Flow cytometry. The lymphocytes in the whole blood samples were stained with FITC- conjugated anti-CD4 and APC-conjugated anti-CD25 antibodies for 15 min at RT. Subsequently, samples were permeabilized with Foxp3 fixation/membrane-breaking working solution (Thermo Fisher Scientific, Inc.; cat. no. 00-5523-00) for 30 min at 4˚C, centrifuged at 500 x g for 5 min at RT and resuspended in PBS. The samples were then incubated with IL-17 PE and Foxp3 PE antibodies (Table II) for 30 min at 4˚C. Cells were detected and analyzed using the Agilent NovoCyte Advanteon flow cytometer (Agilent Technologies, Inc.) controlled by NovoExpress software (v1.5.8; Agilent Technologies, Inc.). The data were analyzed with NovoExpress software.

Histological analysis. The synovial tissues were fixed with 4% paraformaldehyde (PFA) at RT for 48 h, then dehydrated in increasing concentrations of ethanol, made transparent

with xylene and embedded in paraffin wax. Sections of 4 μm thickness were prepared, dewaxed and hydrated prior to being stained. Sections were individually stained with a H&E staining kit and a safranin-O/fast green staining kit. The histological changes were observed under a DM4000B LED light microscope (Leica Microsystems GmbH).

Immunohistochemistry. The synovial tissues were fixed at room temperature for 48 h in 4% PFA, and then dehydrated, permeabilized, embedded in paraffin and sliced into 4-μm-thick sections. After dewaxing and hydration in descending alcohol series, the paraffin sections were incubated with pepsin (2 mg/ml in Tris-HCl; Fuzhou Maixin Biotechnology Development Co., Ltd.; cat. no. DIG-3009) 37˚C for 30 min antigen retrieval. Paraffin sections were incubated with 3% hydrogen peroxide to block endogenous peroxidase activity at RT. After 10 min, the sections were washed with PBS for 3 min three times and blocked with 5% BSA (Wuhan Boster Biological Technology, Ltd.; cat. no. AR0004) for 2 h at RT. The primary antibodies against MCP-1, ICAM-1 and MMP-13 (Table II) were added, and the samples were incubated for 1 h at RT. The sections were subsequently incubated with the HRP conjugated secondary antibody for 30 min using EliVision™ plus kits (cat. no. KIT-9901; Fuzhou Maixin Biotechnology Development Co., Ltd.) at RT. Subsequently the samples were stained with DAB for 5-10 min and hematoxylin for 40 sec at RT. The slices were observed, imaged under a light microscope and analyzed with ImageJ 24.0 software (National Institutes of Health).

Immunofluorescence. Paraffin sections were blocked after dewaxing and hydration as aforementioned. Then, the samples were incubated with primary antibodies against NF-κB p52 and RelB (Table II) overnight at 4˚C. Subsequent incubation with AcalephFluor555 conjugated secondary antibodies (1:500; Cohesion Biosciences; cat. nos. CSA3411 and CSA3408) was performed. Nuclear staining was achieved using DAPI at RT for 10 min. The slices were observed under a fluorescence microscope. The number of positive cells was analyzed via ImageJ 24.0 software.

Western blot analysis. The nuclear extracts were obtained using a commercially available kit (Nanjing KeyGen Biotech Co., Ltd.; cat. no. KGB5302-100), and total proteins were extracted from MH7A cells and tissue using RIPA buffer (Beyotime Institute of Biotechnology; cat. no. P0013B). The protein concentration was measured using a bicinchoninic acid kit (Wuhan Boster Biological Technology, Ltd.; cat. no. AR0146). Protein (30 μg/lane) was subsequently separated via 10% SDS-PAGE and then transferred to nitrocellulose membranes. After blocking with 5% skim milk at RT for 70 min, the membranes were incubated with the primary antibody (Table II) at 4˚C overnight, then the HRP-conjugated secondary antibody (1:5,000; Cell Signaling Technology, Inc. cat. nos. 7074S and 7076S) at RT for 70 min. Enhanced chemiluminescence (Dalian Meilun Biology Technology Co., Ltd.; cat. no. MA0186-1) was used to visualize the immunoblot signals. The grey value of each band was analyzed by ImageJ 24.0 software.

Surface plasmon resonance (SPR). SPR assays were conducted via a BiacoreT200 system (GE Healthcare), following previously established methods (24). Briefly, the Fn14 protein (Sino Biological, Inc.; cat. no. 10431-H01H) was immobilized on a Biacore Sensor Chip CM5 (GE Healthcare). A range of Kir concentrations from 0.0625 μM to 0.032 mM were systematically injected over the immobilized Fn14. The interaction mode and kinetic constant of Kir with Fn14 were established via a 1:1 kinetic model with Biacore Insight (GE Healthcare).

Statistical analysis. The results are expressed as the mean ± SD and were statistically analyzed via SPSS 26.0 (IBM Corp.). Normality was assessed using the Shapiro-Wilk test. For normally distributed data, one-way ANOVA was employed to evaluate differences among multiple groups. Post-hoc analysis was then performed using the Tukey test for data with equal variances and the Games-Howell method for data with unequal variances. For datasets with skewed distributions, the non-parametric statistical method, Kruskal-Wallis test followed by Dunn's post hoc test was applied for multiple comparisons. $P<0.05$ was considered to indicate a statistically significant difference.

Results

Therapeutic effect of Kir on CIA rats. The CIA rat model was successfully established, as demonstrated by the significant increase in both AI [H-value (H)=25.285; degrees of freedom (df)=5; $P<0.01$] and paw edema [F-value (F) (5,54)=6.278; $P<0.01$] in the CIA group compared with the control group (day 1 of treatment). Pre is a commonly prescribed corticosteroid used to manage symptoms of RA. Both treatment with Kir and Pre led to notable reductions in arthritic injury and swelling. Specifically, the AI was significantly decreased on days 10 and 14 ($P<0.01$) in Kir groups. Furthermore, paw edema was significantly diminished from day 7 ($P<0.05$ or $P<0.01$) in the Kir groups (Fig. 2A-C). The serum RF levels were significantly elevated [F(5,54)=33.039; $P<0.01$] in the CIA group compared with the control, and treatment with both Kir and Pre resulted in a notable decrease in serum RF levels in CIA rats ($P<0.01$) (Fig. 2D).

H&E staining showed that the synovial cells in the control group formed a single, organized layer with intact structural integrity. Synovial cells of the CIA rats exhibited a disordered arrangement and increased proliferation, resulting in multiple cell layers. Interspersed among these cells, an increase in inflammatory cells (aggregated nuclei were deep blue) was observed. Furthermore, blood vessels in the synovial tissue showed signs of dilation and congestion. Both treatments with Kir and Pre demonstrated varying levels of effectiveness in reducing synovial tissue hyperplasia and inflammatory cell infiltration (Fig. 2E).

The results of safranin-O/fast green staining showed that the surface of cartilage in the ankle joint was smooth and stained red in the control group. While in the CIA group, notable ankle joint pathology was observed, characterized by structural disorganization, compromised joint integrity, marked erosion and lesions of the red cartilage matrix as well as synovial invasion into the cartilage. Nevertheless, both the Kir and Pre treatments abrogated the loss of chondrocytes

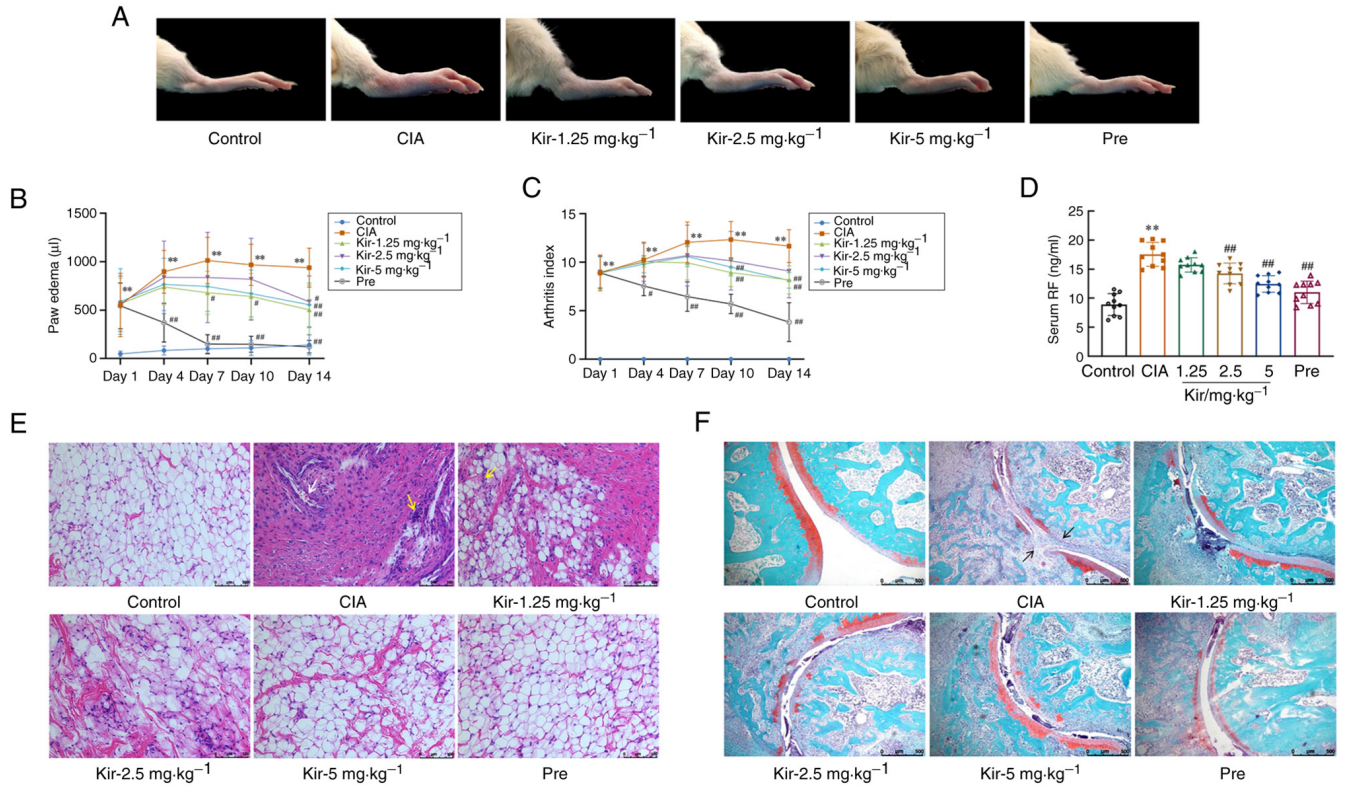

Figure 2. Ameliorative effects of Kir on rheumatoid arthritis in CIA rats. (A) Foot swelling of the rats in each group after Kir intervention. (B) Paw edema of the rats in each group. (C) AI of the rats in each group. (D) RF levels in the serum of the rats in each group. (E) Histopathological changes in the synovial tissue in the rat joints (H&E staining; magnification, x200); the white arrows indicate vascular dilation and congestion and the yellow arrows indicate inflammatory cell infiltration. (F) Histopathological changes of the cartilage tissue in the rat joints (safranin-O/fast staining; magnification, x50); cartilage tissue is stained in red and bone tissue in green; black arrows indicate the invasion of synovial tissue and articular cartilage destruction. All data are expressed as the mean ± SD (n=10). Kruskal-Wallis followed by Dunn's post-test was performed in C, one-way ANOVA followed by Tukey test was performed in D and one-way ANOVA followed by Games-Howell method in B. **P<0.01 vs. the control group; $^{\#}$P<0.05, $^{\#\#}$P<0.01 vs. the CIA group. Kir, Kirenol; CIA, collagen-induced arthritis; AI, arthritis index; RF, rheumatoid factor; H&E, hematoxylin and eosin; Pre, prednisone.

and relieved the damage of the morphological structure (Fig. 2F).

Effect of Kir on the immune inflammatory response in CIA rats. The expression of MCP-1 (H=20.286; df=4; P<0.01), ICAM-1 [F(4,20)=12.269; P<0.01], MMP-13 [F(4,20)=32.440; P<0.01], C-X-C motif chemokine receptor 3 [CXCR3; F(4,20)=7.670; P<0.01] and CXCL-10 [F(4,20)=3.012; P<0.05] in the synovial tissue of the CIA rats was significantly elevated compared with the control. After Kir treatment, the expression of MCP-1, ICAM-1, MMP-13, CXCR3 and CXCL-10 in the synovial tissue of CIA rats was significantly reduced (P<0.05 or P<0.01) (Fig. 3).

The T helper 17 cells (Th17)/regulatory T cell (Treg) ratio [F(4,20)=20.109; P<0.01; Fig. 4E] was significantly elevated in the CIA group, with a notable increase in Th17 cells [F(4,20)=15.854; P<0.01] and a corresponding decrease in Tregs [F(4,20)=5.621; P<0.01]. The CIA group exhibited a marked increase in serum IL-17 levels [F(4,20)=18.324; P<0.01; Fig. 4G], accompanied by a corresponding decrease in IL-10 levels [F(4,20)=9.217; P<0.01; Fig. 4F]. Following Kir treatment, the Th17 level and Th17/Treg ratio decreased significantly (P<0.01), while the Treg level elevated significantly (P<0.05). Additionally, a significant reduction in IL-17 levels and an increase in IL-10 levels were observed (P<0.05 or P<0.01), suggesting a potential therapeutic effect of Kir on immune dysregulation associated with CIA (Fig. 4).

Effects of Kir on the proliferation and migration of MH7A cells. The CCK-8 results indicated that Kir treatment did not significantly affect MH7A cell viability at concentrations ranging from 5 to 80 μM [F(5,24)=0.655; P>0.05; Fig. 5A]. Stimulation with TGF-β1 resulted in aberrant proliferative activity in MH7A cells. Compared with cells in the control group, MH7A cells induced with TGF-β1 presented a significantly greater proliferation rate [F(5,24)=5.849; P<0.01], as determined by the CCK-8 assay. However, compared with the TGF-β1 group, treatment with 5 μM Kir and Pre significantly suppressed the proliferation of MH7A cells (P<0.05) (Fig. 5B).

TGF-β1 stimulation also significantly increased the migratory capacity of MH7A cells [F(5,24)=11.909; P<0.01] compared with the control. However, treatment with Kir and Pre significantly reduced this increase in migration compared with the TGF-β1 group (P<0.01). Considering these findings, along with the previously observed inhibition of Kir on TGF-β1-induced cell proliferation, 5 μM Kir was chosen for subsequent experiments (Fig. 5C and D).

Direct binding interaction between Kir and Fn14. SPR analysis revealed a concentration-dependent binding interaction between Kir and Fn14, with a maximum response of 16 response units (Fig. 6A). The dissociation constant was determined to be 1.2 μM (Fig. 6B).

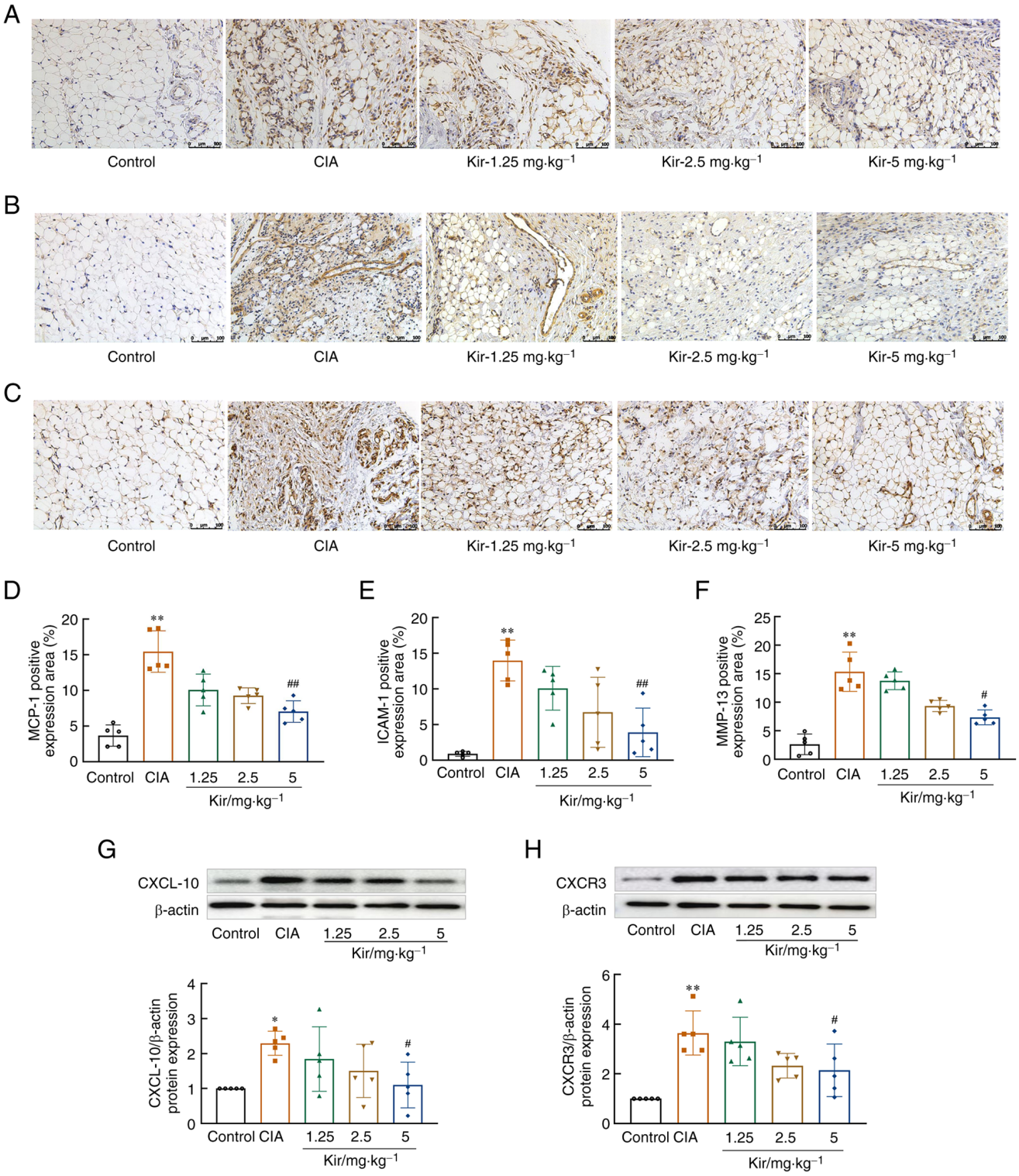

Figure 3. Kir inhibits inflammatory factors and MMP-13 in the synovial tissues of CIA rats. Representative immunohistochemical images of (A) MCP-1, (B) ICAM-1 and (C) MMP-13 in the synovial tissues of various rats (magnification, x200). Quantitative analysis of the immunohistochemistry of (D) MCP-1, (E) ICAM-1 and (F) MMP-13 in the synovial tissues of various groups of rats. Representative images and quantification of the western blot results of (G) CXCL-10 and (H) CXCR3 protein expression. All data are expressed as the mean ± SD (n=5). Kruskal-Wallis with Dunn's post-test was performed in D, one-way ANOVA with Games-Howell method in E and F and one-way ANOVA followed by Tukey test was performed in G and H. *P<0.05, **P<0.01 vs. the control group; $^{\#}$P<0.05, $^{\#\#}$P<0.01 vs. the CIA group. Kir, Kirenol; CIA, collagen-induced arthritis; MCP-1, monocyte chemoattractant protein-1; ICAM-1, intercellular cell adhesion molecule-1; MMP-13, matrix metalloproteinases 13; CXCL-10, C-X-C motif chemokine ligand-10; CXCR3, C-X-C motif chemokine receptor 3.

Effect of Kir on MH7A cells with Fn14-OE. Fn14 overexpression was achieved by lentiviral overexpression vectors, and transduction efficiency was monitored by GFP fluorescence (Fig. 7A). Fn14 overexpression at the protein level was also confirmed by western blotting (Fig. 7B). The aforementioned experiments demonstrated that treatment with 5 μM Kir significantly inhibited both the proliferation and migration of TGF-β1-stimulated MH7A cells. Further analysis demonstrated

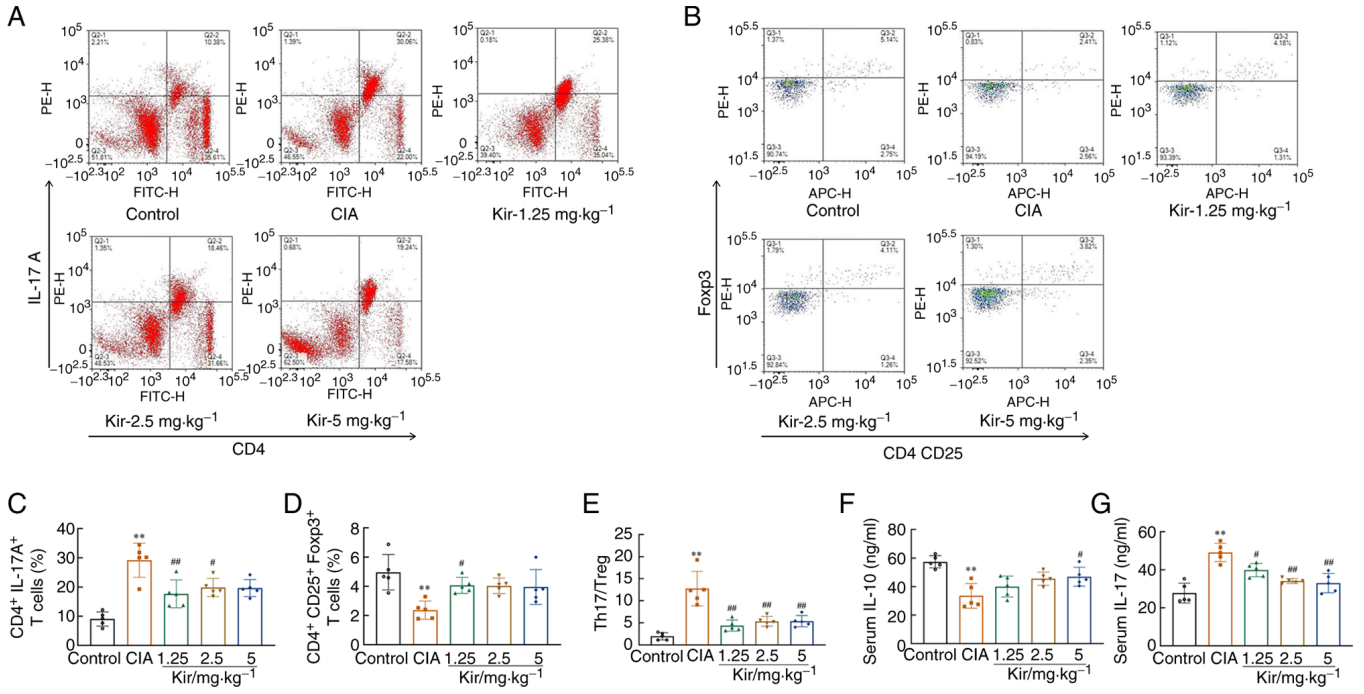

Figure 4. Kir mediates the differentiation of CD4+ T cells in CIA rats. (A) Representative flow cytometry charts of $CD4^+IL\text{-}17^+$ cells in peripheral blood. (B) Representative flow cytometry charts of $CD4^+CD25^+Foxp3^+$ Treg cells in peripheral blood. (C) Flow cytometric analysis of the proportion of $Th17^+$ cells. (D) Flow cytometric analysis of the proportion of Treg cells. (E) The ratios of Th17/Treg cells in peripheral blood were analyzed. (F) IL-10 and (G) IL-17 levels in serum were determined via ELISA. All the data are expressed as the mean ± SD (n=5). One-way ANOVA followed by Tukey test was performed in all analyses. $^{**}P<0.01$ vs. the control group; $^{\#}P<0.05$, $^{\#\#}P<0.01$ vs. the CIA group. Kir, Kirenol; CIA, collagen-induced arthritis; Th17, T helper cell 17; IL-17, interleukin 17; IL-10, interleukin 10.

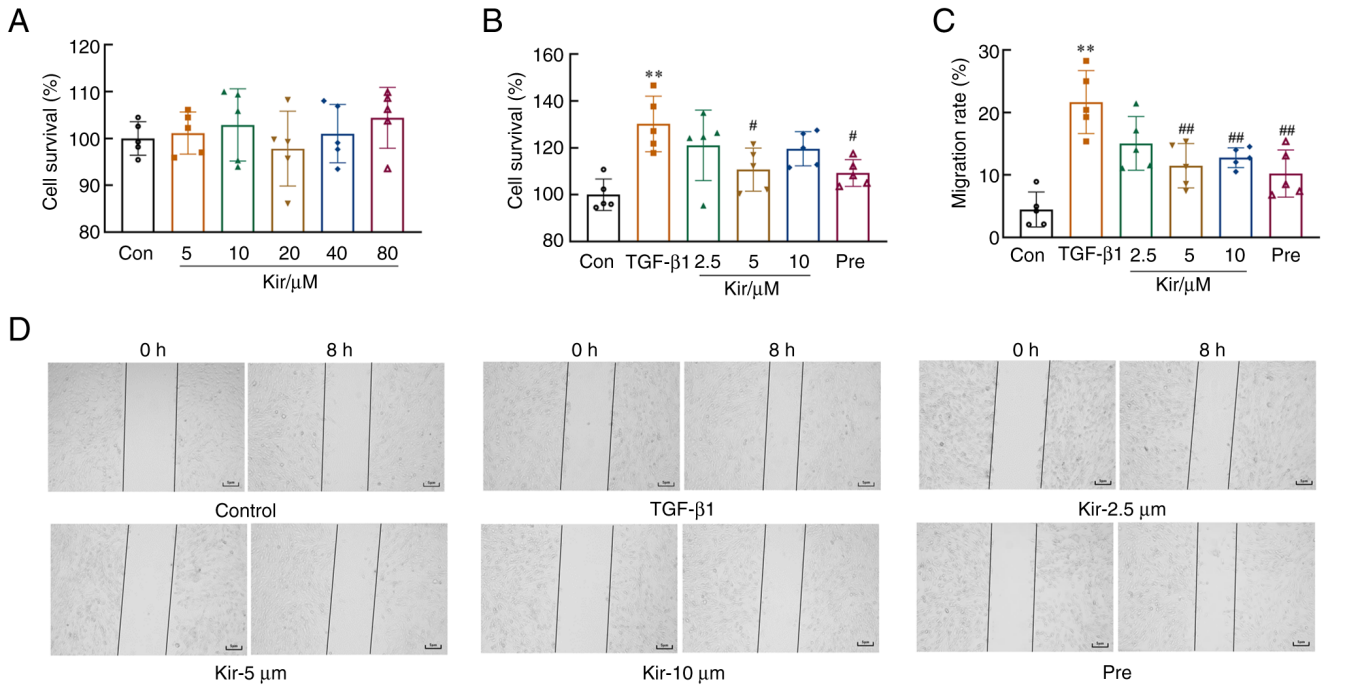

Figure 5. Kir attenuates the proliferation and migration of TGF-β1-induced MH7A cells. (A) Viability of MH7A cells treated with different concentrations of Kir. (B) Effects of Kir on the TGF-β1-induced proliferation of MH7A cells. (C and D) Effects of Kir on the TGF-β1-mediated migration of MH7A cells (magnification, x50). All data are expressed as the mean ± SD (n=5). One-way ANOVA followed by Tukey test was performed in all analyses. $^{**}P<0.01$ vs. the control group; $^{\#}P<0.05$, $^{\#\#}P<0.01$ vs. the TGF-β1 group. Kir, Kirenol; TGF-β1, transforming growth factor-β1.

that overexpression of Fn14 significantly increased both cell proliferation and migration compared with the Kir group ($P<0.05$; Fig. 7C-E).

Compared with the control group, the levels of MCP-1 [$F(4,20)=31.565$; $P<0.01$], ICAM-1 [$F(4,20)=31.514$; $P<0.01$], MMP-13 [$F(4,20)=14.119$; $P<0.01$] and CXCL-10

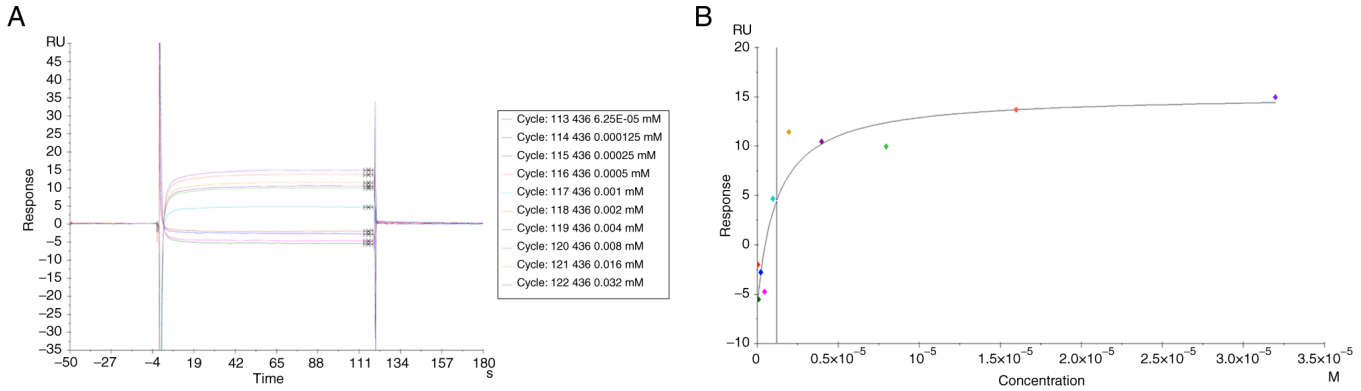

Figure 6. Surface plasmon resonance measurement of the binding between Kir and Fn14. (A) Sensorgram of Kir binding to the Fn14-immobilized chip. (B) The fitted curve for different concentrations of Kir bound to immobilized Fn14. Kir, Kirenol; Fn14, fibroblast growth factor-inducible immediate-early response protein 14; RU, response unit.

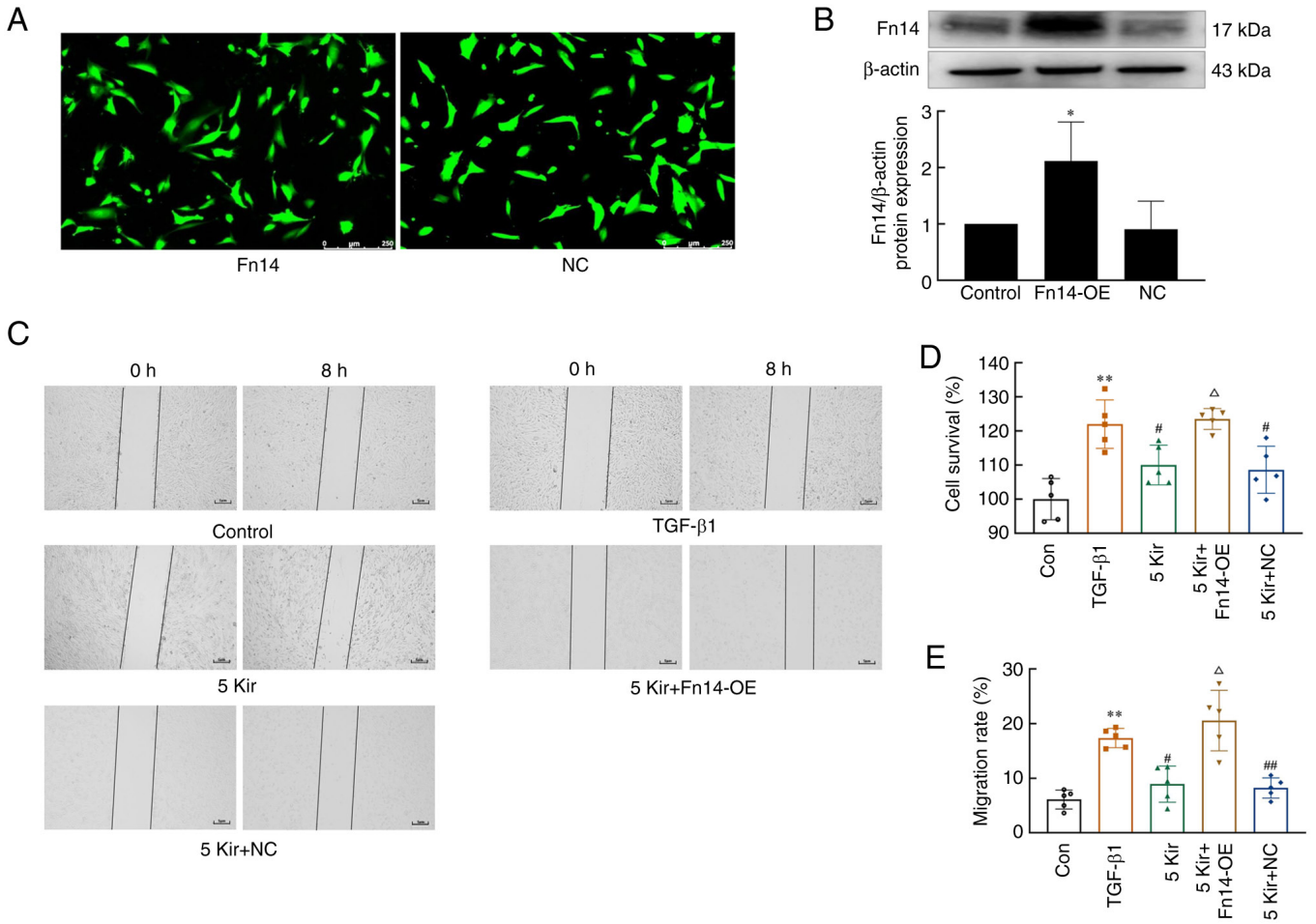

Figure 7. Fn14 overexpression abolishes the effect of Kir on the proliferation and migration of TGF-β1-induced MH7A cells. (A) The GFP expression in MH7A cells transfected with the lentivirus (magnification, x200). (B) The Fn14 protein levels in MH7A cells transfected with Fn14-OE compared with NC lentivirus; β-actin was used as normalization control; (n=3) *P<0.05 vs. NC group. (D) Effect of Kir on the proliferation of Fn14-overexpressing MH7A cells. (C and E) Effect of Kir on the migratory ability of Fn14-overexpressing MH7A cells (magnification, x50); (n=5). One-way ANOVA followed by LSD was performed in B, one-way ANOVA followed by Tukey test was performed in D and one-way ANOVA followed by Games-Howell was performed in F. **P<0.01 vs. the control group, $^{\#}$P<0.05 or $^{\#\#}$P<0.01 vs. the TGF-β1 group, $^{\triangle}$P<0.05 vs. the 5 μM Kir group. All the data are expressed as the mean ± SD. Kir, Kirenol; TGF-β1, transforming growth factor-β1. Kir, Kirenol; Fn14, fibroblast growth factor-inducible immediate-early response protein 14; Fn14-OE, Fn14-overexpressing lentivirus; NC, negative control; Con, control.

[F(4,20)=71.270; P<0.01] increased significantly in the TGF-β1 stimulated MH7A cell supernatant. Treatment with 5 μM Kir significantly reduced these elevated levels (P<0.05 or P<0.01). However, Fn14 overexpression resulted in the abrogation of the effects produced by 5 μM Kir (P<0.05 or P<0.01) (Fig. 8).

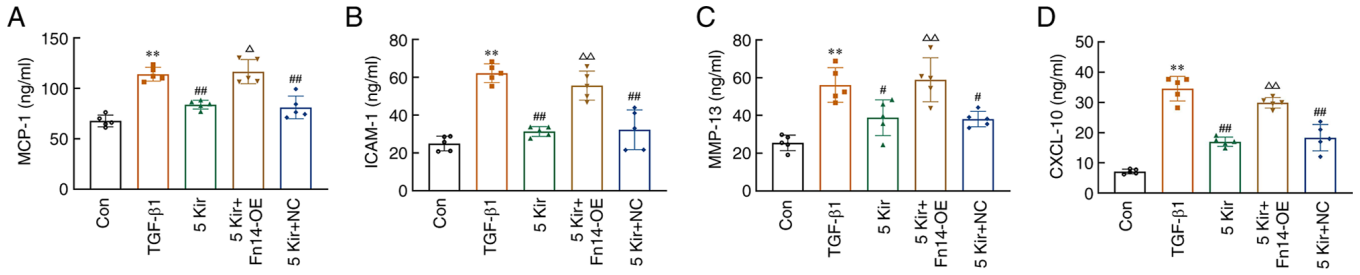

Figure 8. Fn14 overexpression blocks the effects of Kir on chemokines and MMP-13 in TGF-β1-induced MH7A cells. Levels of (A) MCP-1, (B) ICAM-1, (C) MMP-13 and (D) CXCL-10 in the cell supernatant of MH7A cells. All the data are expressed as the mean ± SD (n=5). One-way ANOVA followed by Tukey test was performed in C and one-way ANOVA followed by Games-Howell in A, B and D. **P<0.01 vs. the control group, $^{\#}$P<0.05 or $^{\#\#}$P<0.01 vs. the TGF-β1 group, $^{\triangle}$P<0.05 or $^{\triangle\triangle}$P<0.01 vs. the 5 μM Kir group. Fn14, fibroblast growth factor-inducible immediate-early response protein 14; Kir, kirenol; MCP-1, monocyte chemoattractant protein-1; ICAM-1, intercellular cell adhesion molecule-1; MMP-13, matrix metalloproteinases 13; CXCL10, C-X-C motif chemokine ligand 10.

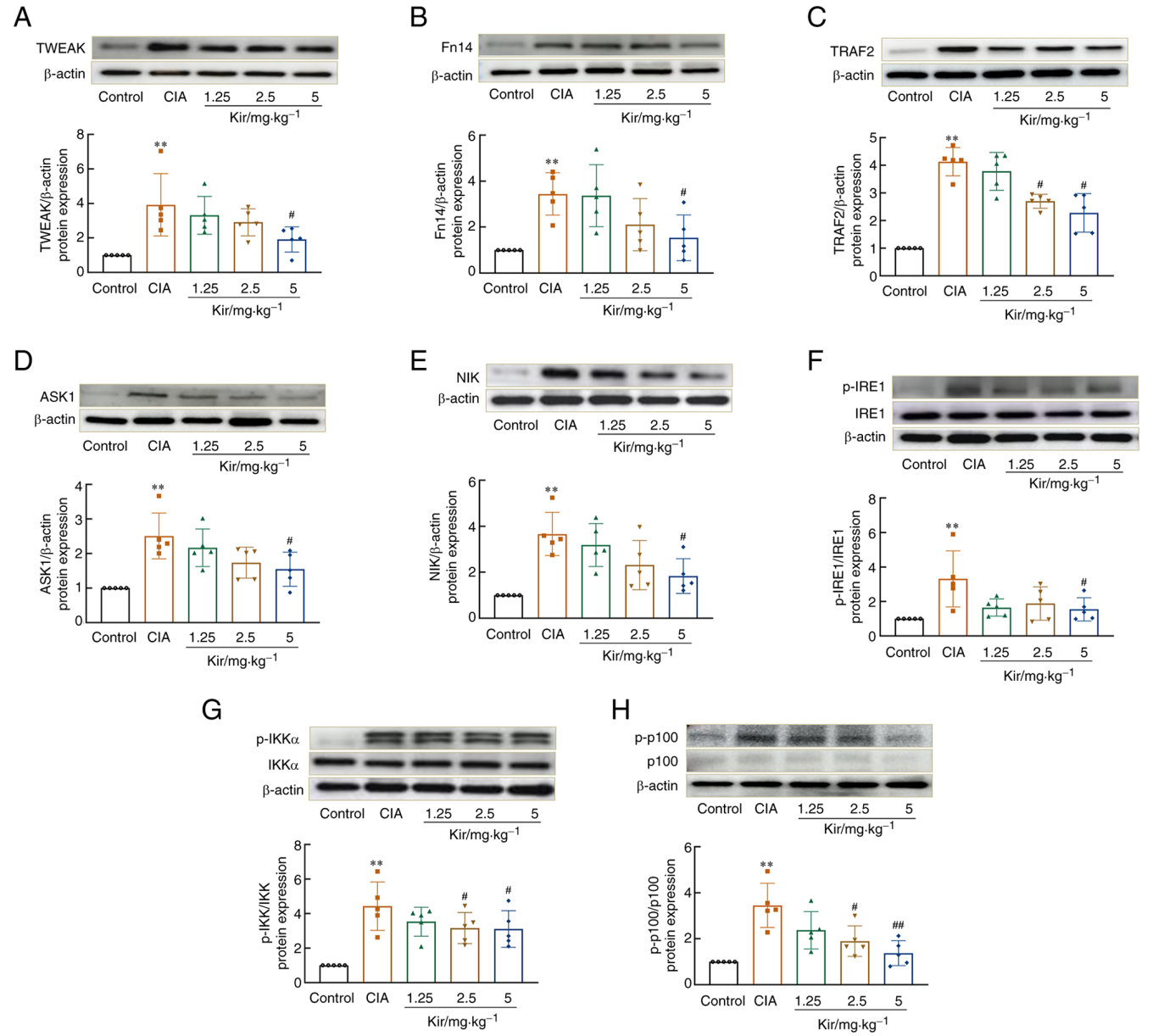

Figure 9. Kir attenuates the levels of TWEAK/Fn14 pathway-associated proteins in the synovial tissues of CIA rats. Representative western blots and quantification of the (A) TWEAK, (B) Fn14, (C) TRAF2, (D) ASK1 and (E) NIK protein levels and the phosphorylation of (F) IRE1, (G) IKKα and (H) p100. β-actin was used as the loading control. All the data are expressed as the mean ± SD (n=5). Kruskal-Wallis followed by Dunn's post-test was performed in D, one-way ANOVA followed by Games-Howell in C and one-way ANOVA followed by Tukey test was performed in A, B and E-H. **P<0.01 vs. the control group, $^{\#}$P<0.05 or $^{\#\#}$P<0.01 vs. the CIA group. Fn14, fibroblast growth factor-inducible immediate-early response protein 14; Kir, kirenol; CIA, collagen-induced arthritis; TWEAK, tumor necrosis factor-like weak inducer of apoptosis; NIK, nuclear factor-κB-inducing kinase; IRE1, inositol-requiring enzyme 1; IKKα, inhibitor of κB kinase α.

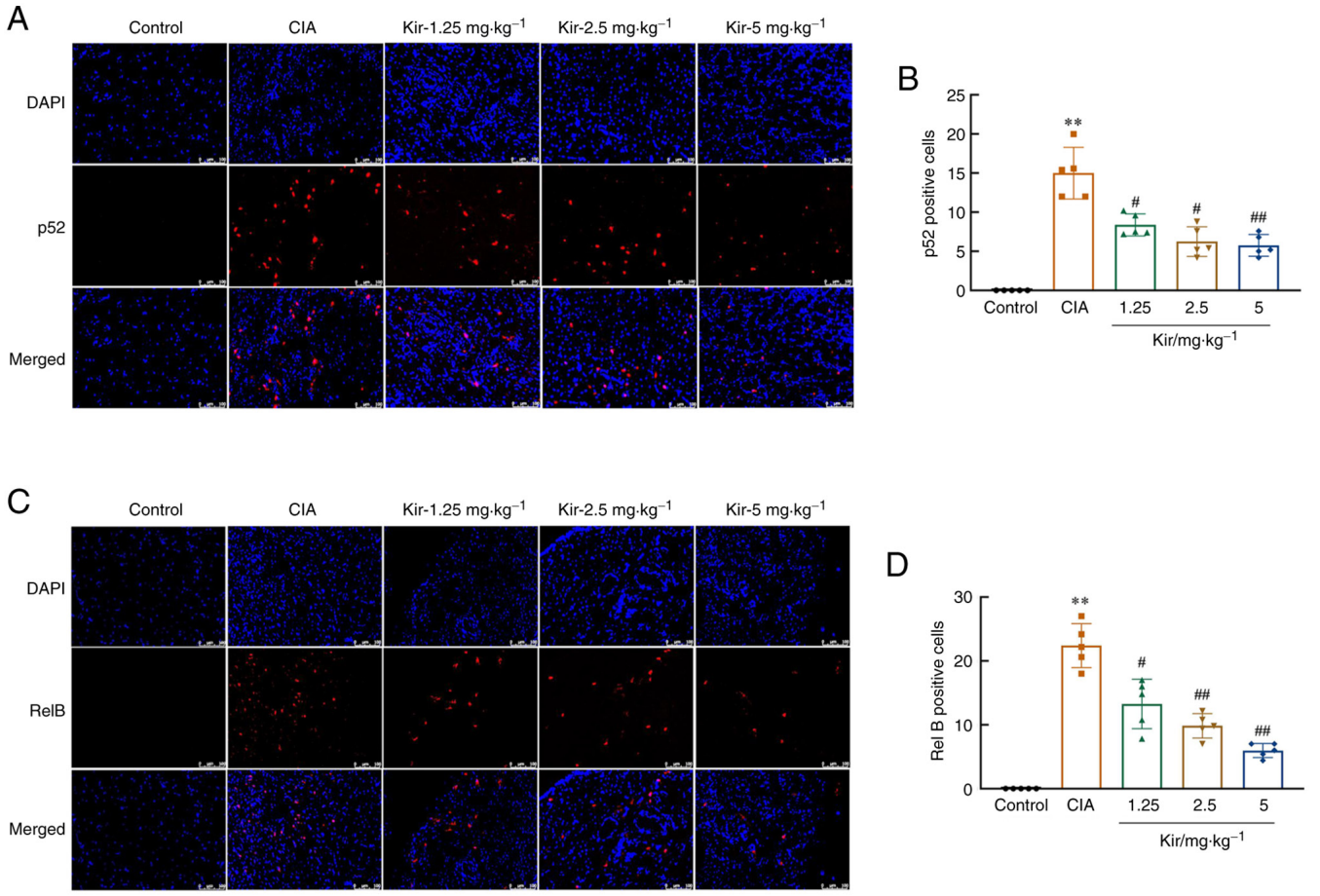

Figure 10. Kir reduces nuclear localization of p52 and RelB in the synovial tissues of CIA rats. (A) Representative images of immunofluorescence staining for p52 protein in the nucleus (magnification, x200). (B) Quantitative analysis of nuclear p52 protein. (C) Representative images of immunofluorescence staining for RelB proteins in the nucleus (magnification, x200); (D) Quantitative analysis of nuclear RelB protein. All the data are expressed as the mean ± SD (n=5). One-way ANOVA with Games-Howell method was performed for all analyses. **P<0.01 vs. the control group, $^{\#}$P<0.05 or $^{\#\#}$P<0.01 vs. the CIA group. Kir, kirenol; CIA, collagen-induced arthritis; PCNA, proliferating cell nuclear antigen.

Kir attenuates the TWEAK/Fn14 pathway in vitro and in vivo. Studies revealed significant upregulation of the TWEAK/Fn14 signaling pathway in the synovial tissues of CIA rats. Western blot analysis demonstrated increased expression of TWEAK [F(4,20)=5.083; P<0.01], Fn14 [F(4,20)=5.926; P<0.01] and its downstream signaling proteins, TNF receptor-associated factor 2 [TRAF2; F(4,20)=30.392; P<0.01], apoptosis signal-regulating kinase 1 [ASK1; H=15.278; df=4; P<0.01] and NF-κB-inducing kinase [NIK; F(4,20)=8.120; P<0.01] in the synovial tissues of CIA rats compared with control rats. The levels of inositol-requiring enzyme 1 [IRE1; F(4,20)=4.381, P<0.01], inhibitor of κB kinase α [IKKα; F(4,20)=8.626; P<0.01] and p100 phosphorylation [F(4,20)=9.829; P<0.01] were significantly elevated (P<0.01) (Fig. 9) in the CIA group compared with the Control group. Additionally, immunofluorescence staining revealed that the number of cells positive for p52 [F(4,20)=39.743; P<0.01] and RelB [F(4,20)=55.329; P<0.01] nucleation was significantly greater in CIA rats compared with the control group (Fig. 10). Kir treatment resulted in significant downregulation of TWEAK, Fn14, TRAF2, ASK1 and NIK expression and suppressed the phosphorylation of IRE1, IKKα and p100 (P<0.05 or P<0.01) compared with the CIA group. Furthermore, a significant decrease in both p52 and RelB nuclear translation was observed (P<0.05 or P<0.01).

Cellular experiments demonstrated that Kir significantly downregulated the protein expression of TWEAK [F(4,10)=5.497; P<0.05], total Fn14 [F(4,10)=4.469; P<0.05], nuclear p52 [F(4,10)=4.729; P<0.05] and RelB [F(4,10)=9.353; P<0.05] in TGF-β1-stimulated cells, while also inhibiting IKKα [F(4,10)=7.530; P<0.05] and p100 phosphorylation [F(4,10)=4.552; P<0.05]. However, overexpression of Fn14 reversed these effects of Kir (P<0.05) (Fig. 11).

Discussion

CIA is the most prevalent inducible model for RA due to its high success rate in inducing disease and its ability to recapitulate numerous features of human RA, including its pathogenesis and immunological characteristics (25). In the present study, joint inflammation and swelling was assessed by monitoring AI and paw edema in each group of rats. Swelling became evident ~15 days (day 1 of treatment) after the model was established, peaked at 21 days (day 7 of treatment), which aligned with findings reported in the literature (26). CIA rats presented with significantly greater AI scores and paw edema than the control rats. Histological examination of both synovial and ankle joint tissue revealed hallmark pathological changes, including inflammatory cell infiltration, abnormal

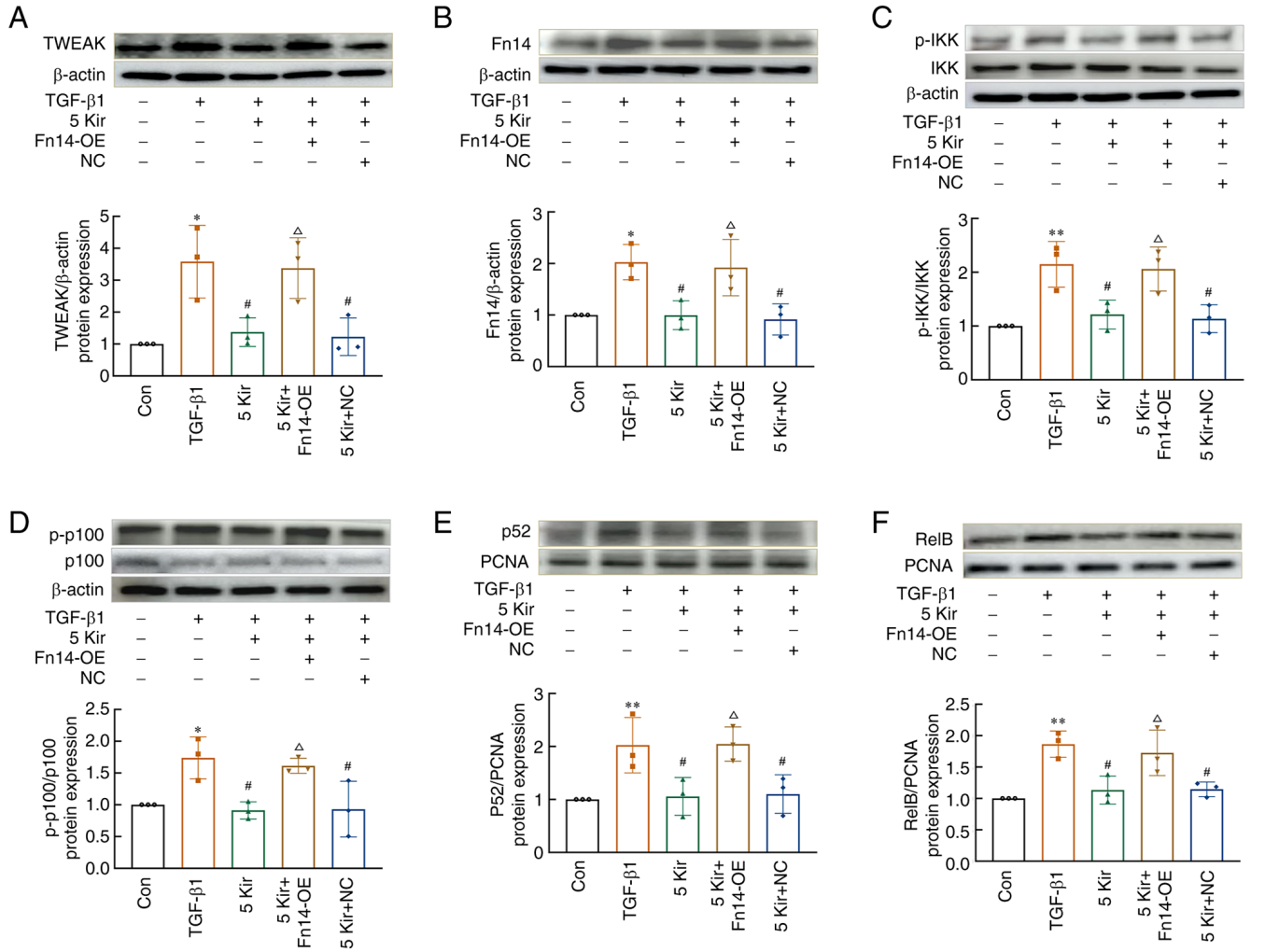

Figure 11. Fn14 overexpression blocks the effect of Kir on TWEAK/Fn14 pathway-related proteins in TGF-β1-induced MH7A cells. Representative images and quantification of western blot results showing the protein expression of (A) TWEAK (B) and Fn14, and the phosphorylation of (C) IKKα and (D) p100. β-actin was used as the loading control. Representative images and quantification of western blot results for the nuclear proteins (E) p52 and (F) RelB. PCNA was used as the loading control for nucleoprotein. All the data are expressed as the mean ± SD (n=3). One-way ANOVA followed by Tukey test was performed in all analyses. *P<0.05 or **P<0.01 vs. the control group, $^{\#}$P<0.05 vs. the TGF-β1 group, $^{\Delta}$P<0.05 vs. the 5 μM Kir group. Kir, kirenol; TGF-β1, transforming growth factor-β1; PCNA, proliferating cell nuclear antigen; TWEAK, tumor necrosis factor-like weak inducer of apoptosis; Fn14, fibroblast growth factor-inducible immediate-early response protein 14; PCNA, proliferating cell nuclear antigen.

cell proliferation and invasion as well as degeneration of articular cartilage, confirming the successful induction of CIA in the experimental model. Kir treatment significantly alleviated joint damage, reduced swelling and ameliorated the pathology in both the synovial and ankle joint tissue of CIA rats. These findings suggest that Kir may exert a significant reparative and protective effect on joint tissue injury and inflammatory infiltration. RF is an autoantibody that binds to the Fc region of denatured IgG, specifically recognizing an antigenic determinant cluster within this fragment (27). Serum RF levels are a significant indicator for the clinical diagnosis of RA (28). In the CIA group, RF levels were significantly elevated. Kir treatment effectively inhibited the production of RF, thereby helping to reduce the joint damage caused by the autoimmune response.

FLSs play a crucial role in RA, driving its pathogenesis through abnormal proliferation, activation and migration. These processes lead to synovial thickening, extracellular matrix (ECM) degradation and ultimately, erosion of articular cartilage and bone, causing irreversible joint damage (29). Inflammation is the central factor driving the relentless progression and deterioration of RA, serving as the primary causative agent for the characteristic symptoms of joint swelling and pain. When RA develops, FLSs undergo excessive proliferation, resulting in a surge of inflammatory chemokines, including MCP-1 and ICAM-1. These chemokines contribute to joint inflammation by recruiting neutrophils and stimulating further synovial cell growth (30,31). MMPs are a highly conserved class of proteases. Under pathological conditions, activated FLSs release large amounts of MMPs, leading to irreversible degradation of the ECM in articular cartilage, increased FLS invasiveness and accelerated destruction of cartilage and bone (32). MMP-13, which has the highest efficiency in degrading collagen type II and is the dominant component of articular cartilage, is considered the rate-limiting enzyme for cartilage destruction (33,34). The findings of the present study revealed significantly elevated levels of MCP-1, ICAM-1 and MMP-13 in both synovial tissue and TGF-β1-induced MH7A

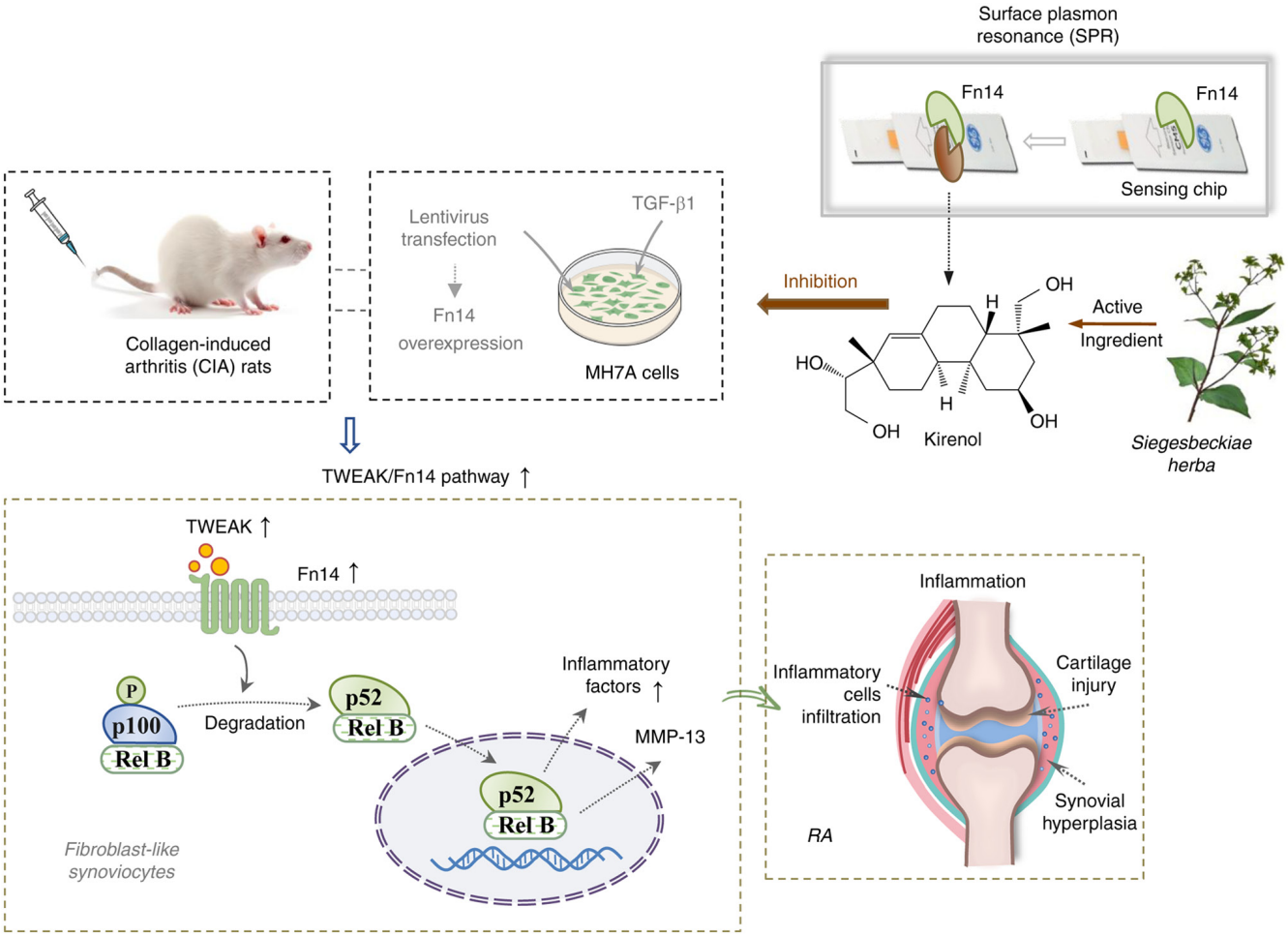

Figure 12. Kir relieves rheumatoid arthritis-induced synovial cell injury via modulation of the TWEAK/Fn14 signaling pathway *in vivo* and *in vitro*. TWEAK, tumor necrosis factor-like weak inducer of apoptosis; Fn14, fibroblast growth factor-inducible immediate-early response protein 14; RA, rheumatoid arthritis; NIK, nuclear factor-κB-inducing kinase; IKKα, inhibitor of κB kinase α; MCP-1, monocyte chemoattractant protein-1; ICAM-1, intercellular cell adhesion molecule-1; MMP-13, matrix metalloproteinases 13; CXCL10, C-X-C motif chemokine ligand 10; C-X-C motif chemokine receptor 3; IL-17, interleukin 17; IL-10, interleukin 10.

cells. Kir treatment effectively reduced the secretion of these inflammatory markers, mitigating the inflammatory response and decreasing the number of invasive FLSs both *in vivo* and *in vitro*.

Th cells constitute a major subset of adaptive immune cells responsible for coordinating immune responses. The development of RA is significantly influenced by a dysregulation in the balance between Th17 and Tregs (35). Th17 cells contribute to inflammation by releasing IL-17, driving the infiltration of immune cells into the synovium and promoting the proliferation of FLSs. Conversely, Tregs suppress inflammation and maintain immune homeostasis by producing the anti-inflammatory cytokine IL-10 (36). Chemokines are key immunomodulatory molecules that mediate the activation and movement of inflammatory cells to synovial tissues (37,38). CXCR3, a G-protein-coupled chemokine receptor expressed by Th cells, interacts with its ligand, CXCL-10, leading to both the chemotaxis of effector T cells to inflammatory sites and Th17 differentiation (39,40). This shift in the Th17/Treg cell balance further promotes excessive immune-inflammatory responses (41). In the present study, flow cytometry analysis revealed significant increases in Th17 cell populations, the Th17/Treg ratio, serum IL-17 levels and CXCL-10 and CXCR3 protein expression in CIA rats. Conversely, Treg populations and serum IL-10 levels were significantly decreased. These findings indicate that CXCL-10 and CXCR3 upregulation disrupts the Th17/Treg balance in the context of RA. Kir treatment effectively regulated the Th17/Treg balance in RA by downregulating CXCL-10/CXCR3 expression, suppressing IL-17 production and promoting IL-10 production. These effects may ultimately inhibit the aberrant immune-inflammatory response associated with RA.

Research has revealed a crucial role for the TWEAK/Fn14 signaling pathway in RA. Specifically, upon RA onset, TWEAK is activated and its expression is upregulated. TWEAK, via its extracellular C-terminus, undergoes trimerization and then binds to its receptor, Fn14, inducing Fn14 trimerization. This process leads to the recruitment of the downstream target molecule, TRAF2, to the cytoplasm. TRAF2, with its E3 ubiquitin ligase activity, interacts with IRE1 (42,43), promoting IRE1 phosphorylation. This activated IRE1 recruits ASK1, leading to NIK activation, which subsequently phosphorylates IKKα, ultimately activating the p52/RelB NF-κB non-canonical pathway (44,45). p52 is degraded from its precursor protein

p100, which forms a complex with RelB. This complex is inactive due to the presence of an inhibitory structural domain at the C-terminus of p100, which prevents the nuclear localization and activation of RelB (46). When IKKα is phosphorylated, p100 undergoes phosphorylation at serine 672, leading to its processing into p52. This processing removes the inhibitory domain at the C-terminus of p100, exposing the nuclear localization sequence of p52. The p52 protein then forms a heterodimer with RelB, which translocates to the nucleus. RelB, which contains transcriptionally active domains, binds to the promoters of relevant inflammatory factors, chemokines and other genes, initiating their transcription and expression (47). In the present study, the results of the SPR analysis revealed a specific interaction between Kir and Fn14. *In vivo* studies revealed that Kir significantly reduced the expression of TWEAK, Fn14, TRAF2, ASK1 and NIK in the synovial tissues of CIA rats and decreased the phosphorylation levels of IRE1 and IKKα. These findings support the notion that Kir inhibits the activation of the non-canonical NF-κB pathway.

The activation of the TWEAK/Fn14 signaling pathway is regulated by the expression levels of Fn14, and TGF-β1 has been demonstrated to upregulate the expression of Fn14 (48). In the present study, the inflammatory proliferation of MH7A cells was established through induction by TGF-β1, which was followed by Fn14 overexpression experiments to investigate the molecular mechanisms of Kir. Kir treatment effectively suppressed the TGF-β1-induced abnormal proliferation and migration of MH7A cells. This was accompanied by a significant downregulation of TWEAK and Fn14 protein levels, as well as reduced phosphorylation of IKKα and p100, leading to diminished processing of p100 into p52. Consequently, the expression of downstream factors such as MCP-1, ICAM-1, CXCL-10 and MMP-13 was inhibited. These findings aligned with results from animal experiments. Furthermore, overexpression of Fn14 reversed the inhibitory effects of Kir, highlighting the critical role of Fn14 in mediating the effects of this compound.

The present study investigated the role and mechanism of Kir in suppressing synovial hyperplasia during RA progression. In CIA models, Kir was also effectively attenuated cartilage degeneration and synovial pannus formation, suggesting multi-target mechanisms involving angiogenesis suppression and tissue hyperplasia modulation. However, additional molecular targets and associated signaling pathways require further investigation.

Kir demonstrates a high safety profile. In an acute toxicity study in rats, a single oral gavage dose of 5 g/kg Kir (equivalent to 100 times the proposed human clinical dose) resulted in no mortality or abnormal physiological reactions. Furthermore, no toxicological effects were observed during daily administration for 14 consecutive days (21). Pharmacokinetic studies revealed that Kir is absorbed throughout the gastrointestinal tract in rats, with notably improved absorption in intestinal segments. Notably, in the present study, it was also found that Kir administration in rats did not produce gastrointestinal adverse effects (such as diarrhea) observed with prednisone (Pre) therapy during the treatment period. These properties underscore the strong clinical translation potential of Kir. Based on current evidence, Kir demonstrates a good safety profile and is suitable for oral administration in chronic disease management. Current studies on Kir, including the present study, remain predominantly confined to preclinical models, such as animal studies and *in vitro* cell systems. While these approaches provide valuable mechanistic insights, differences in drug processing and immune systems between species also limit direct application to patients. Thus, further studies are required to investigate the effectiveness, safe dosage and long-term safety of Kir in humans.

In summary, the present study demonstrated that Kir exhibits anti-RA activity by targeting the TWEAK/Fn14 signaling pathway. Kir inhibits the activation of this pathway, leading to the downregulation of downstream target genes and the modulation of the Th17/Treg balance, all of which contribute to a reduction in abnormal immune inflammatory responses (Fig. 12). These actions lead to decreased proliferation and invasiveness of synovial cells, ultimately mitigating pathological damage. Kir is a potential candidate drug for RA treatment. These results not only validate historical herb applications but also suggest potential for modern drug derived from natural products.

Acknowledgements

Not applicable.

Funding

This work was supported by the National Natural Science Foundation of China (grant no. 82204378), the Science Foundation of the Fujian Province (grant no. 2022J01864) and the School Fund of Fujian University of Traditional Chinese Medicine (grant no. X2019007-Professional).

Availability of data and materials

The data generated in the present study may be requested from the corresponding author.

Authors' contributions

ZXC and LX substantially contributed to the experimental conception and design of the study. ZHC and WL contributed to the acquisition of data and analysis of *in vitro* experiments. ZXC, JW, ZHC and LX contributed to the acquisition of data and analysis of the animal experiments. WX, YL and MH contributed to statistical analysis and visualization. YZ, YW and LN analyzed the results and reviewed the manuscript. YC edited the manuscript, interpretated the data and acquired funding. YC and LN confirm the authenticity of all the raw data. All authors have read and approved the final version of the manuscript.

Ethics approval and consent to participate

Ethics approval for the animal experiments was obtained from the Animal Ethics Committee of Fujian University of Traditional Chinese Medicine (Fuzhou, China; approval no. FJTCM IACUC 2023008). All animal experiments conducted in the present study followed the guidelines and regulations specified in this ethical approval.

Patient consent for publication

Not applicable.

Competing interests

The authors declare that they have no competing interests.

References

1. Macáková K, Illésová J, Mlynáriková V, Lesayová A, Konečná B, Vlková B, Celec P and Šteňová E: The dynamics of extracellular DNA associates with treatment response in patients with rheumatoid arthritis. Sci Rep 12: 21099, 2022.
2. Weyand CM and Goronzy JJ: The immunology of rheumatoid arthritis. Nat Immunol 22: 10-18, 2021.
3. Modarresi Chahardehi A, Masoumi SA, Bigdeloo M, Arsad H and Lim V: The effect of exercise on patients with rheumatoid arthritis on the modulation of inflammation. Clin Exp Rheumatol 40: 1420-1431, 2022.
4. Finckh A, Gilbert B, Hodkinson B, Bae SC, Thomas R, Deane KD, Alpizar-Rodriguez D and Lauper K: Global epidemiology of rheumatoid arthritis. Nat Rev Rheumatol 18: 591-602, 2022.
5. Nii T, Maeda Y, Motooka D, Naito M, Matsumoto Y, Ogawa T, Oguro-Igashira E, Kishikawa T, Yamashita M, Koizumi S, *et al*: Genomic repertoires linked with pathogenic potency of arthritogenic *Prevotella copri* isolated from the gut of patients with rheumatoid arthritis. Ann Rheum Dis 82: 621-629, 2023.
6. Garcia-Carbonell R, Divakaruni AS, Lodi A, Vicente-Suarez I, Saha A, Cheroutre H, Boss GR, Tiziani S, Murphy AN and Guma M: Critical role of glucose metabolism in rheumatoid arthritis fibroblast-like synoviocytes. Arthritis Rheumatol 68: 1614-1626, 2016.
7. Gao X, Kang X, Lu H, Xue E, Chen R, Pan J and Ma J: Piceatannol suppresses inflammation and promotes apoptosis in rheumatoid arthritis-fibroblast-like synoviocytes by inhibiting the NF-κB and MAPK signaling pathways. Mol Med Rep 25: 180, 2022.
8. Nygaard G and Firestein GS: Restoring synovial homeostasis in rheumatoid arthritis by targeting fibroblast-like synoviocytes. Nat Rev Rheumatol 16: 316-333, 2020.
9. van Kuijk AW, Wijbrandts CA, Vinkenoog M, Zheng TS, Reedquist KA and Tak PP: TWEAK and its receptor Fn14 in the synovium of patients with rheumatoid arthritis compared to psoriatic arthritis and its response to tumour necrosis factor blockade. Ann Rheum Dis 69: 301-304, 2010.
10. Rodríguez-Muguruza S, Altuna-Coy A, Castro-Oreiro S, Poveda-Elices MJ, Fontova-Garrofé R and Chacón MR: A serum biomarker panel of exomiR-451a, exomiR-25-3p and soluble TWEAK for early diagnosis of rheumatoid arthritis. Front Immunol 12: 790880, 2021.
11. Kamijo S, Nakajima A, Kamata K, Kurosawa H, Yagita H and Okumura K: Involvement of TWEAK/Fn14 interaction in the synovial inflammation of RA. Rheumatology (Oxford) 47: 442-450, 2008.
12. Park JS, Park MK, Lee SY, Oh HJ, Lim MA, Cho WT, Kim EK, Ju JH, Park YW, Park SH, *et al*: TWEAK promotes the production of interleukin-17 in rheumatoid arthritis. Cytokine 60: 143-149, 2012.
13. Drosos AA, Pelechas E, Kaltsonoudis E and Voulgari PV: Therapeutic options and cost-effectiveness for rheumatoid arthritis treatment. Curr Rheumatol Rep 22: 44, 2020.
14. Crofford LJ: Use of NSAIDs in treating patients with arthritis. Arthritis Res Ther 15 Suppl 3 (Suppl 3): S2, 2013.
15. Radu AF and Bungau SG: Management of rheumatoid arthritis: An overview. Cells 10: 2857, 2021.
16. Jiang Z, Yu QH, Cheng Y and Guo XJ: Simultaneous quantification of eight major constituents in Herba Siegesbeckiae by liquid chromatography coupled with electrospray ionization time-of-flight tandem mass spectrometry. J Pharm Biomed Anal 55: 452-457, 2011.
17. Ibrahim SRM, Altyar AE, Sindi IA, El-Agamy DS, Abdallah HM, Mohamed SGA and Mohamed GA: Kirenol: A promising bioactive metabolite from siegesbeckia species: A detailed review. J Ethnopharmacol 281: 114552, 2021.
18. Lu Y, Xiao J, Wu ZW, Wang ZM, Hu J, Fu HZ, Chen YY and Qian RQ: Kirenol exerts a potent anti-arthritic effect in collagen-induced arthritis by modifying the T cells balance. Phytomedicine 19: 882-889, 2012.
19. Wang ZM, Zhu SG, Wu ZW, Lu Y, Fu HZ and Qian RQ: Kirenol upregulates nuclear annexin-1 which interacts with NF-κB to attenuate synovial inflammation of collagen-induced arthritis in rats. J Ethnopharmacol 137: 774-782, 2011.
20. Hu W, Mao C and Sheng W: The protective effect of kirenol in osteoarthritis: An in vitro and in vivo study. J Orthop Surg Res 17: 195, 2022.
21. Lu S: Anti-rheumatic drug Kirenol's preparations and reasearch. Master thesis. Guangzhou University of Chinese Medicine, 2014 (In Chinese).
22. Nan LH, Liu YF, Huang M, Xu W, Li H, Chu KD and Yang L: Effects of *Tripterygium wilfordii* Hook. F. before and after processing on CIA model rats. Chin J Tradit Chin Med Pharm 35: 5795-5799, 2020 (In Chinese).
23. Han L, Zhang XZ, Wang C, Tang XY, Zhu Y, Cai XY, Wu YJ, Shu JL, Wang QT, Chen JY, *et al*: IgD-Fc-Ig fusion protein, a new biological agent, inhibits T cell function in CIA rats by inhibiting IgD-IgDR-Lck-NF-κB signaling pathways. Acta Pharmacol Sin 41: 800-812, 2020.
24. Liu YJ, Xu WH, Fan LM, Zhang YQ, Xu W, Chen YP, Chen LL, Chen L, Xu W, Wang Y, *et al*: Polydatin alleviates DSS- and TNBS-induced colitis by suppressing Th17 cell differentiation via directly inhibiting STAT3. Phytother Res 36: 3662-3671, 2022.
25. Asquith DL, Miller AM, McInnes IB and Liew FY: Animal models of rheumatoid arthritis. Eur J Immunol 39: 2040-2044, 2009.
26. Chen J, Che Q, Kou Y, Rong X, Zhang X, Li M and Shu Q: A novel drug combination of Tofacitinib and Iguratimod alleviates rheumatoid arthritis and secondary osteoporosis. Int Immunopharmacol 124: 110913, 2023.
27. Togashi T, Ishihara R, Watanabe R, Shiomi M, Yano Y, Fujisawa Y, Katsushima M, Fukumoto K, Yamada S and Hashimoto M: Rheumatoid factor: Diagnostic and prognostic performance and therapeutic implications in rheumatoid arthritis. J Clin Med 14: 1529, 2025.
28. Steiner G and Toes REM: Autoantibodies in rheumatoid arthritis-rheumatoid factor, anticitrullinated protein antibodies and beyond. Curr Opin Rheumatol 36: 217-224, 2024.
29. Chen Y, Han T, Guo Z, Li X, Zhang X and Peng W: Editorial: Immunomodulatory roles of fibroblast-like synoviocytes in rheumatoid arthritis. Front Immunol 15: 1415672, 2024.
30. Cho ML, Yoon BY, Ju JH, Jung YO, Jhun JY, Park MK, Park SH, Cho CS and Kim HY: Expression of CCR2A, an isoform of MCP-1 receptor, is increased by MCP-1, CD40 ligand and TGF-beta in fibroblast like synoviocytes of patients with RA. Exp Mol Med 39: 499-507, 2007.
31. Zhao S, Wang Y, Hou L, Wang Y, Xu N and Zhang N: Pentraxin 3 inhibits fibroblast growth factor 2 induced osteoclastogenesis in rheumatoid arthritis. Biomed Pharmacother 131: 110628, 2020.
32. Jia Q, Wang T, Wang X, Xu H, Liu Y, Wang Y, Shi Q and Liang Q: Astragalin suppresses inflammatory responses and bone destruction in mice with collagen-induced arthritis and in human fibroblast-like synoviocytes. Front Pharmacol 10: 94, 2019.
33. Li H, Wang D, Yuan Y and Min J: New insights on the MMP-13 regulatory network in the pathogenesis of early osteoarthritis. Arthritis Res Ther 19: 248, 2017.
34. Hu Q and Ecker M: Overview of MMP-13 as a promising target for the treatment of osteoarthritis. Int J Mol Sci 22: 1742, 2021.
35. Paradowska-Gorycka A, Wajda A, Romanówska-Prochnicka K, Walczuk E, Kuca-Warnawin E, Kmiolek T, Stypinska B, Rzeszotarska E, Majewski D, Jagodzinski PP and Pawlik A: Th17/Treg-related transcriptional factor expression and cytokine profile in patients with rheumatoid arthritis. Front Immunol 11: 572858, 2020.
36. Gautam S, Kumar R, Kumar U, Kumar S, Luthra K and Dada R: Yoga maintains Th17/Treg cell homeostasis and reduces the rate of T cell aging in rheumatoid arthritis: A randomized controlled trial. Sci Rep 13: 14924, 2023.
37. Godessart N and Kunkel SL: Chemokines in autoimmune disease. Curr Opin Immunol 13: 670-675, 2001.
38. Iwamoto T, Okamoto H, Toyama Y and Momohara S: Molecular aspects of rheumatoid arthritis: Chemokines in the joints of patients. FEBS J 275: 4448-4455, 2008.
39. Groom JR and Luster AD: CXCR3 in T cell function. Exp Cell Res 317: 620-631, 2011.

40. Christen U, McGavern DB, Luster AD, von Herrath MG and Oldstone MB: Among CXCR3 chemokines, IFN-gamma-inducible protein of 10 kDa (CXC chemokine ligand (CXCL) 10) but not monokine induced by IFN-gamma (CXCL9) imprints a pattern for the subsequent development of autoimmune disease. J Immunol 171: 6838-6845, 2003.
41. Li J, Ge M, Lu S, Shi J, Li X, Wang M, Huang J, Shao Y, Huang Z, Zhang J, *et al*: Pro-inflammatory effects of the Th1 chemokine CXCL10 in acquired aplastic anaemia. Cytokine 94: 45-51, 2017.
42. Siegmund D, Zaitseva O and Wajant H: Fn14 and TNFR2 as regulators of cytotoxic TNFR1 signaling. Front Cell Dev Biol 11: 1267837, 2023.
43. Madhavan A, Kok BP, Rius B, Grandjean JMD, Alabi A, Albert V, Sukiasyan A, Powers ET, Galmozzi A, Saez E and Wiseman RL: Pharmacologic IRE1/XBP1s activation promotes systemic adaptive remodeling in obesity. Nat Commun 13: 608, 2022.
44. Lin CC, Lin WN, Cho RL, Wang CY, Hsiao LD and Yang CM: TNF-α-induced $cPLA_2$ expression via NADPH oxidase/reactive oxygen species-dependent NF-κB cascade on human pulmonary alveolar epithelial cells. Front Pharmacol 7: 447, 2016.
45. O'Dea E and Hoffmann A: NF-κB signaling. Wiley Interdiscip Rev Syst Biol Med 1: 107-115, 2009.
46. Sun SC: Non-canonical NF-κB signaling pathway. Cell Res 21: 71-85, 2011.
47. Lawrence T: The nuclear factor NF-kappaB pathway in inflammation. Cold Spring Harb Perspect Biol 1: a001651, 2009.
48. Dohi T and Burkly LC: The TWEAK/Fn14 pathway as an aggravating and perpetuating factor in inflammatory diseases: Focus on inflammatory bowel diseases. J Leukoc Biol 92: 265-279, 2012.